JOURNAL OF AIRCRAFT
Vol. 45, No. 1, January–February 2008

Maneuver Load Analysis of Overdetermined Trim Systems

Daniella E. Raveh*
Technion—Israel Institute of Technology, 32000 Haifa, Israel

DOI: 10.2514/1.29118

A new method for computational fluid dynamics-based maneuver trim optimization is presented, in which the aircraft is trimmed by using the angle-of-attack, tail deflection, and wing control surfaces. The method belongs to the category of closely coupled aeroelastic analyses, in which the flow analysis, elastic deformations, and trim optimization computations are embedded within the computational fluid dynamics code, and performed within a single run. The method is tested on a maneuvering fighterlike aircraft model in a 1-*g* level flight, at Mach 0.5, sea level, and a 5-*g* pull-up maneuver, at Mach 0.8, sea level. The trim algorithm is found to be robust, and the closely coupled approach is computationally efficient. The newly proposed methodology provides a tool for computing loads on a maneuvering realistic aircraft, in both traditional maneuver trim, and when wing control surfaces are used. It can be used to compute nonlinear maneuver loads, in the transonic flight regime, for structural design, and to gain insight on control laws that can be applied to reduce maneuver loads on existing aircrafts.

Introduction

MANEUVER loads play a key part in the design of aircraft structure, as a large portion of the airframe is designed to bear these loads, to meet strength, static aeroelastic effectiveness, and dynamic aeroelastic requirements [1]. Out of the myriad of loading cases examined, the structure is designed to meet critical maneuvers, which are often associated with transonic flight conditions and nonlinear flows. The long-established use of linear aerodynamic methods for maneuver-load analysis necessitates supporting the design and certification processes with extensive wind-tunnel and flight testing. Accurate load estimates typically become available in late stages of the design process, resulting in design modifications that are mandatory for adequate flight clearance [2,3]. Accurate estimation of maneuver loads becomes more challenging and prominent when multiple control surfaces are used to trim the aircraft. This is the case of the active aeroelastic wing (AAW) technology, in which redundant control surfaces are used on a flexible wing to provide maneuver-load control, increased roll authority, or decreased maneuver drag [4–8]. With AAW technology, maneuver loads affects both the structural design and the design of control laws, and thus their accurate estimation is vital [9].

Maneuver trim analysis requires the coupling of the structural inertial, the elastic, and the aerodynamic forces. Two approaches exist for this coupling, namely, the loosely coupled and the tightly coupled analyses. In the loosely coupled approach the flow solver and structural solver use segregated tools. That is, the aerodynamic forces are computed by the computational fluid dynamics (CFD) solver, separately from the elastic forces, which are computed by the structural solver. An interface tool is needed to link the two disciplinary solvers. An example of the loosely coupled approach is a load analysis study of an F-16 model in a max-*g* pull-up, by Love et al. [10]. In this study, Lockheed's SPLITFLOW unstructured CFD code was used together with the MSC/NASTRAN finite element code, and the multidisciplinary computing environment (MDICE) code [11] that was used to transfer data between these disciplinary modules. Other examples include load analysis of an A340-like aircraft, by Heinrich et al. [12], based on the unstructured TAU CFD code, NASTRAN, and MpCCI interface method, and a static aeroelastic simulation of the X-31A research wing by Stettner et al. [13]. The loosely coupled approach is attractive for complex configuration analysis, because it allows for the use of existing and validated, or commercial, disciplinary solvers. Its main hindrances are the large computational resources and large run times required for each analysis, partially attributed to the massive data transfer between the CFD and structural disciplinary codes.

The closely coupled approach computes both the flowfield and the elastic forces and deformations within the CFD solver. A structural solver is used to compute the structure's stiffness properties, which are then read into the CFD solver. An iterative process of computing aerodynamic loads, applying them to the structure, deforming the CFD mesh and recomputing aerodynamic loads is performed within the CFD solver. This eliminates the need for an interface tool, and significantly cuts down the data transfer between solvers. Trim analysis requires another iterative process, in which the trim parameters are adjusted until the aircraft is trimmed.

A review of early works of closely coupled CFD-based static aeroelasticity analyses can be found in [14]. Among the more recent works are the studies by Schuster et al. [15,16], based on the Lockheed Euler/Navier–Stokes aerodynamic code ENS3D, Guruswamy [17], and Obayashi and Guruswamy [18] based on the ENSAERO solver coupled with a finite element beam-type structural model. These studies present static aeroelastic analysis at fixed flight conditions. Raveh et al. [19,20] presented a CFD-based trim analysis, based on an in-house CFD solver and a NASTRAN modal model. The applications in all of these studies were very basic. None involved control surface deflections or overdetermined trim systems. Generally speaking, none of the closely coupled maneuver schemes described in the literature presented a realistic trimmed load analysis of a maneuvering aircraft.

The current study investigates the evolvement of CFD tools for trim analysis of both traditional and overdetermined trim systems. A "traditional" trim system is a determined system, in which the number of trim parameters equals the number of trim degrees of freedom, whereas in an overdetermined system, the number of trim parameters is larger than the number of trim degrees of freedom. The latter is the case of AAW technology, and it calls for an optimization scheme to replace the closed-form solution of the determined trim system. The current study deals with the implementation of trim optimization schemes within a CFD flow solver. It focuses on issues of flow analysis of deflected control surfaces, convergence and computational efficiency of the trim scheme, the computation of sensitivities for the optimization, and the application to a realistic fighterlike aircraft model.

Received 1 December 2006; revision received 24 May 2007; accepted for publication 24 May 2007.

*Senior Lecturer, Faculty of Aerospace Engineering. Member AIAA.

Methodology

Static Aeroelastic Maneuver Trim Analysis

The static aeroelastic equation of a free aircraft in discrete finite element degrees of freedom is

$$[K]\{u\} + [M]\{\ddot{u}\} = \{F_A\} \tag{1}$$

where $[K]$ and $[M]$ are the stiffness and mass matrices, $\{u\}$ is the vector of structural displacements, which include rigid-body translations and rotations, plus elastic deformations, and $\{F_A\}$ is the vector of aerodynamic forces. The linear aerodynamic method typically expresses the aerodynamic forces as the sum of rigid forces due to the aerodynamic trim parameters, plus elastic force increments due to elastic structural deformations. The latter term is dependent on the structural displacements $\{u\}$, and is thus returned to the left-hand side of Eq. (1) as an aerodynamic stiffness term. In the current approach, in which the aerodynamic forces on the elastic aircraft are computed by an elastic CFD analysis, the rigid and elastic parts are nonseparable, and the vector $\{F_A\}$ comprises the aerodynamic forces on the elastically deformed aircraft.

Using the modal approach, the structural displacements are written as a linear combination of the free aircraft's rigid-body modes, $[\phi_R]$, and a few of its low frequency elastic modes, $[\phi_E]$:

$$\{u\} = [\,\phi_R \quad \phi_E\,]\begin{Bmatrix}\xi_R\\ \xi_E\end{Bmatrix} \tag{2}$$

where $\{\xi_R\}$ and $\{\xi_E\}$ are the rigid-body and elastic generalized displacements, respectively. The typical number of elastic modes that has to be accounted for in trim analysis is on the order of a few tens. A parametric study of the number of modes required for trim and structural optimization of the specific test case of this study is presented in [21].

Equation (1), in generalized coordinates, reads

$$\begin{bmatrix}M_{RR} & M_{RE}\\ M_{ER} & M_{EE}\end{bmatrix}\begin{Bmatrix}\ddot{\xi}_R\\ \ddot{\xi}_E\end{Bmatrix} + \begin{bmatrix}K_{RR} & K_{RE}\\ K_{ER} & K_{EE}\end{bmatrix}\begin{Bmatrix}\xi_R\\ \xi_E\end{Bmatrix} = \begin{Bmatrix}F_{AR}\\ F_{AE}\end{Bmatrix} \tag{3}$$

where

$$[M_{RR}] = [\phi_R]^T[M][\phi_R] \qquad [M_{EE}] = [\phi_E]^T[M][\phi_E] \tag{4a}$$

and

$$[M_{ER}] = [M_{RE}]^T = [\phi_E]^T[M][\phi_R] = 0 \tag{4b}$$

due to the orthogonality of the rigid-body and elastic modes of the free aircraft.

$$[K_{EE}] = [\phi_E]^T[K][\phi_E] \tag{5a}$$

$$[K_{ER}] = [K_{RE}]^T = [\phi_E]^T[K][\phi_R] = 0 \tag{5b}$$

due to mode orthogonality, and

$$[K_{RR}] = [\phi_R]^T[K][\phi_R] = 0 \tag{5c}$$

This last relation reflects the fact that there are no elastic forces associated with rigid-body motion.

$$\{F_{AR}\} = [\phi_R]^T\{F_A\} \tag{6a}$$

$$\{F_{AE}\} = [\phi_E]^T\{F_A\} \tag{6b}$$

Substituting Eqs. (4–6) into Eq. (3) and assuming that the elastic accelerations are negligible compared to the rigid-body maneuver accelerations, the static aeroelastic equation can be written as two decoupled equations, one for the rigid body and one for the elastic motion:

$$[M_{RR}]\{\ddot{\xi}_R\} = \{F_{AR}\} \tag{7}$$

$$[K_{EE}]\{\xi_E\} = \{F_{AE}\} \tag{8}$$

Equation (7) is solved for the aerodynamic trim parameters, that is, angle of attack (AOA), sideslip angle, control surface deflections, and rotation rates that trim the aircraft to a maneuver prescribed by the rigid-body accelerations. As stated previously, elasticity effects are included in the generalized force vector $\{F_{AR}\}$. Equation (8) is solved for the elastic deformations pertaining to the aerodynamic trim parameters and flight conditions.

Equations (7) and (8) are computed in the CFD analysis in an iterative manner, as proposed by Raveh et al. [22] and shown in Fig. 1. The CFD analysis starts with an initial guess of the trim parameters. A user-defined number of iterations are performed to compute the flowfield on the rigid configuration. Then, a subroutine is called that calculates the generalized aerodynamic forces associated with the elastic modes [Eq. (6b)], and another subroutine solves Eq. (8) for the elastic deformations. The CFD grid is deformed to reflect the elastically deformed aircraft shape, based on the elastic part of Eq. (2), $\{u_E\} = [\phi_E]\{\xi_E\}$. The method for mapping the elastic modes from the finite element nodes in which they are computed to the CFD surface nodes and the method for grid stretching following each elastic deformation are described in [22]. The process of computing elastic deformations and then recomputing the forces on the deflected configuration is repeated to convergence. It yields the elastic forces associated with a specific set of aerodynamic trim parameters.

For trimmed maneuvers an outer iterative loop is introduced that solves Eq. (7). Namely, it searches for a set of aerodynamic trim parameters that balances Eq. (7) for a user-defined rigid-body accelerations vector. For a symmetric maneuver Eq. (7) can be stated as two equations of balance of the lift and pitching moment:

$$\begin{aligned}&\sum_{i=1}^{n_{cs}}(C_{L_{\delta_i}})_{\text{flex}}\Delta\delta_i + (C_{L_\alpha})_{\text{flex}}\Delta\alpha + L_0/(qS) = L_{\text{trim}}/(qS)\\ &\quad = Wn_z/(qS)\\ &\sum_{i=1}^{n_{cs}}(C_{M_{\delta_i}})_{\text{flex}}\Delta\delta_i + (C_{M_\alpha})_{\text{flex}}\Delta\alpha + M_0/(qSc) = M_{\text{trim}}/(qSc) = 0\end{aligned} \tag{9}$$

where L_{trim} is the required trim lift, which equals the aircraft weight W times the load factor n_z, M_{trim} is the trim pitching moment that

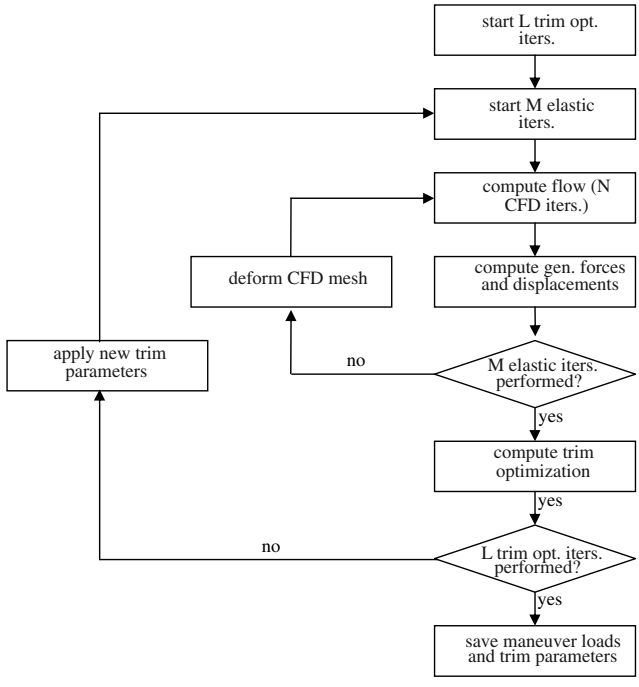

Fig. 1 Flowchart of the trim optimization process.

equals zero, q is the dynamic pressure, and S and c are the reference area and chord, respectively. L_0 and M_0 refer to the flexible lift and moment terms *that correspond to a current set of values of trim parameters*, and $\Delta\alpha$ and $\Delta\delta_i$ are the increments of trim parameters, from their current values, that are required to trim the aircraft. n_{cs} is the number of control surfaces, including the elevator. Angular rates associated with the maneuver can be introduced to the flow analysis by writing the flow equations in a rotating coordinate system. This was not done in this study, and the forces due to angular rates were neglected.

In the case in which the number of aerodynamic trim parameters equals the number of rigid-body modes, Eq. (7) has a closed-form solution. However, if multiple control surfaces are used to trim the aircraft, the trim system is overdetermined [as in Eq. (9)], and a closed-form solution does not exist. The trim problem must then be formulated as an optimization problem (i.e., trim optimization) to determine the combination of trim parameter values that trim the aircraft and minimize an objective of interest to the analyst.

Overdetermined Trim System

For a symmetric maneuver, the trim optimization problem may be posed as a minimization of the root bending moment (RBM), subject to control surface travel limits, hinge moment (HM) constraints, and trim balance requirements.

Minimize

$$\mathrm{RBM} = \sum_{i=1}^{n_{cs}} \left(\frac{\partial(\mathrm{RBM})}{\partial\delta_i}\right)_{\mathrm{flex}} \Delta\delta_i + \left(\frac{\partial(\mathrm{RBM})}{\partial\alpha}\right)_{\mathrm{flex}} \Delta\alpha + \mathrm{RBM}_0 \tag{10}$$

Subject to

control surface travel limits

$$-10 \text{ deg} \le \delta_{\mathrm{LEI}} \le 10 \text{ deg}, \qquad -10 \text{ deg} \le \delta_{\mathrm{LEO}} \le 10 \text{ deg},$$
$$-10 \text{ deg} \le \delta_{\mathrm{TEI}} \le 10 \text{ deg}, \qquad -10 \text{ deg} \le \delta_{\mathrm{TEO}} \le 10 \text{ deg},$$
$$-10 \text{ deg} \le \delta_{\mathrm{HT}} \le 10 \text{ deg}, \qquad -10 \text{ deg} \le \alpha \le 10 \text{ deg}$$

HM constraints

$$-3.0 \times 10^5 \le \mathrm{HM}_{\mathrm{LEI}} \le 3.0 \times 10^5,$$
$$-1.0 \times 10^5 \le \mathrm{HM}_{\mathrm{LEO}} \le 1.0 \times 10^5,$$
$$-1.5 \times 10^5 \le \mathrm{HM}_{\mathrm{TEI}} \le 1.5 \times 10^5,$$
$$-5.0 \times 10^4 \le \mathrm{HM}_{\mathrm{TEO}} \le 5.0 \times 10^4 \qquad (\mathrm{lb} \cdot \mathrm{in.})$$

where the hinge moment of each control surface is given by

$$\mathrm{HM}_{cs} = \sum_{i=1}^{n_{cs}} \left(\frac{\partial(\mathrm{HM}_{cs})}{\partial\delta_i}\right)_{\mathrm{flex}} \Delta\delta_i + \left(\frac{\partial(\mathrm{HM}_{cs})}{\partial\alpha}\right)_{\mathrm{flex}} \Delta\alpha + \left(\frac{\partial(\mathrm{HM}_{cs})}{\partial n_z}\right)_{\mathrm{flex}} n_z + \mathrm{HM}_{cs0}$$

satisfaction of trim equations (lift and pitching-moment balance)

$$\sum_{i=1}^{n_{cs}} (C_{L_{\delta_i}})_{\mathrm{flex}} \Delta\delta_i + (C_{L_\alpha})_{\mathrm{flex}} \Delta\alpha + L_0/qS = L_{\mathrm{trim}}/qS = Wn_z/qS$$

$$\sum_{i=1}^{n_{cs}} (C_{M_{\delta_i}})_{\mathrm{flex}} \Delta\delta_i + (C_{M_\alpha})_{\mathrm{flex}} \Delta\alpha + M_0/qSc = M_{\mathrm{trim}}/qSc = 0$$

The design variables are as follows: α, δ_{LEI}, δ_{LEO}, δ_{TEI}, δ_{TEO}, and δ_{HT}.

RBM_0 and HM_{cs0} refer to the aerodynamic hinge moments (not including the hinge moment due to inertial forces that is written as a separate term) that correspond to the current setting of trim parameters. The control surface hinge moment limits are based on typical allowables for modern fighter aircraft. Control surface deflections were limited in this study to values that are about a third of typical max deflections. This was done because of the limitation of the Euler solver that cannot process detached flows associated with large deflection angles.

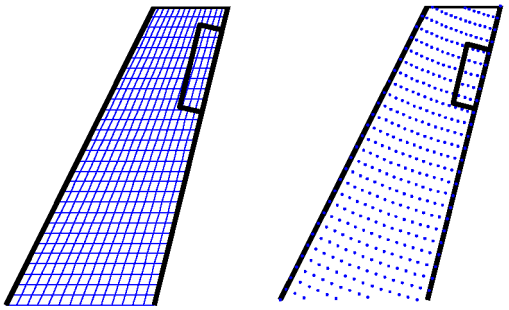

a) b)

Fig. 2 Wing with a flap that does not lie on grid lines.

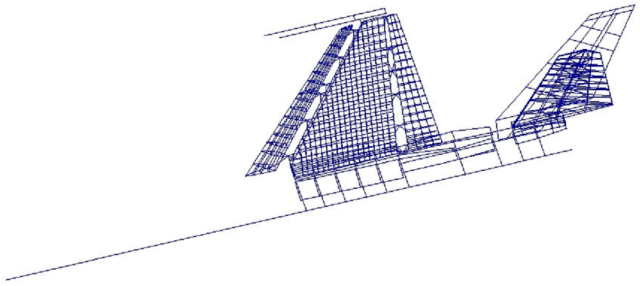

Fig. 3 Structural model of generic fighter.

Trim optimization by Eq. (10) requires the estimation of the sensitivity derivatives of the aerodynamic coefficients, RBM, and HM, with respect to the trim parameters. These derivatives vary from point to point at the parameters space, and they cannot be calculated explicitly. In the current study these derivatives are computed about the zero deflections of all trim parameters. CFD analyses are executed to compute the flowfield at the baseline zero value of trim

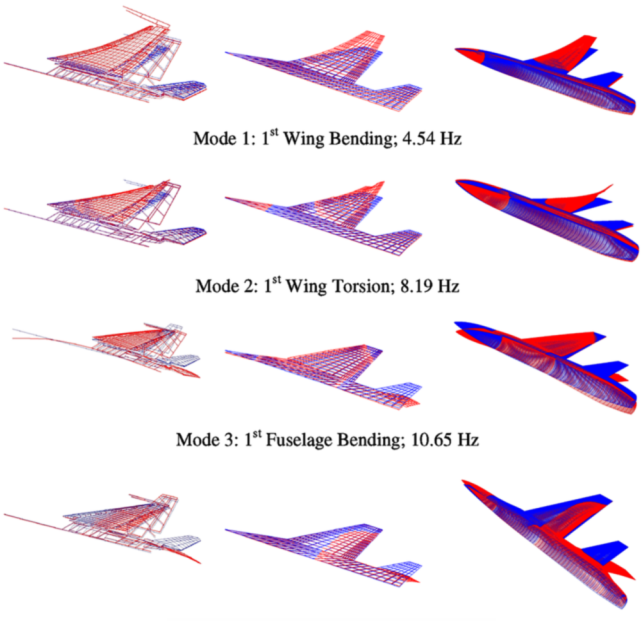

Fig. 4 First four elastic modes used in the trim analysis. Left column: modes in finite element nodes; middle column: modes in linear panel model; right column: modes in CFD surface mesh.

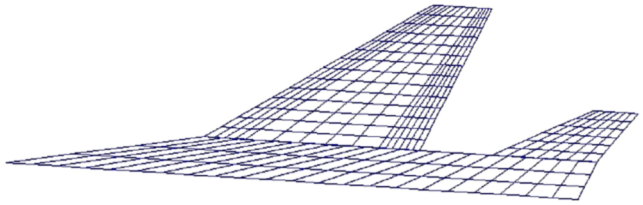

Fig. 5 ZAERO panel aerodynamic model of generic fighter.

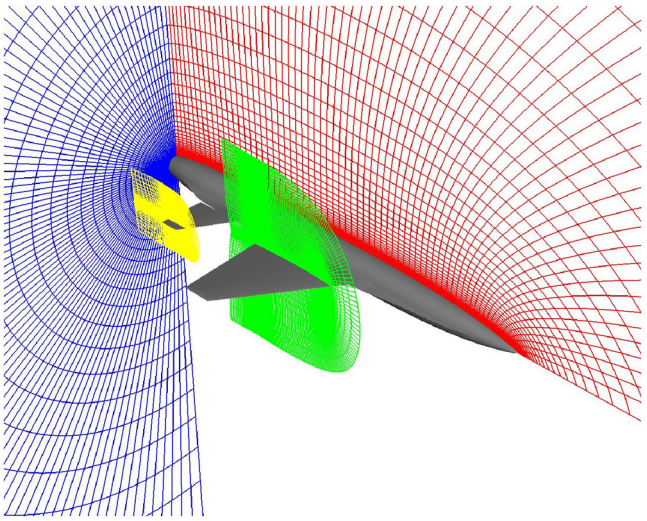

Fig. 6 CFD model of generic fighter.

parameters, and the flowfields associated with a perturbation of each trim parameter, and the sensitivities are computed by finite differencing.

Zink et al. [23] discuss and compare the modified method of feasible directions and the simplex method for trim optimization. The latter is a non-gradient-based algorithm, designed for the solution of linear programs. A linear program is an optimization problem whose objective and constraints (inequality and/or equality) are linear functions of the design variables. One of the features of the simplex method is that convergence to the optimal solution is typically very consistent, meaning that regardless of the starting point, the algorithm will converge to the same solution. The symmetric trim optimization problem, as formulated in Eq. (10), is already cast in the form of a linear program, and the simplex algorithm is used in this study for trim optimization. For the formulation of the antisymmetric trim problem as a linear programming (LP) problem the reader is referred to [23].

Following a trim correction, the variation of the angle of attack is introduced to the CFD flow analysis as an increment to the far-field velocity components. Control surface deflections are introduced by deforming the computational mesh, using control surface modes. The control surface deflection method is presented in the following section.

Flap Deflection

CFD analysis about a wing with deflected flaps raises the problem of modeling flap deflections within the computational grid. A strict approach would aim at modeling the flow through the gap between the wing and the deflected flap. This can be achieved with a Chimera-type grid, in which the wing and the flap are modeled by separate, overlapping grids [24]. Although results demonstrate that this method can accurately predict the wing–flap flow, it requires a tedious grid preparation. An alternative approach neglects the flow through the wing–flap gap and models the wing and deflected flap as one continuous surface, in which the grid lines are bent to represent the deflected flap. This approach was used by Bartels and Schuster [25] in flow analysis of the benchmark active controls technology (BACT) wing. It results in skewed grid lines in the wing–flap boundary region and is thus limited to small deflections. This problem can be somewhat alleviated by condensing grid lines in the wing–flap boundary region, such that the wing–flap gap is represented continuously, over several grid lines. A more stringent limitation of this approach is that it can only be used in wing geometries in which the wing–flap split line lies on grid lines, in the flow direction. In the case of a swept wing, in which the split line is perpendicular to the trailing edge and does not necessarily lie on a grid line in the flow direction, this approach is inadequate. This case is shown in Fig. 2a.

To overcome this problem, the current study uses the infinite plate spline (IPS) method [26] to generate a surface grid for the wing with deflected flaps (see [26] for the IPS implementation). For the

Table 1 Number of grids in each grid zone of the CFD model

	Chordwise	Spanwise	Normal	Total
Fuselage	70	91	53	337,610
Wing	237	63	40	597,240
HT	199	48	30	286,560
Interface	80	65	40	208,000
Total				1,429,410

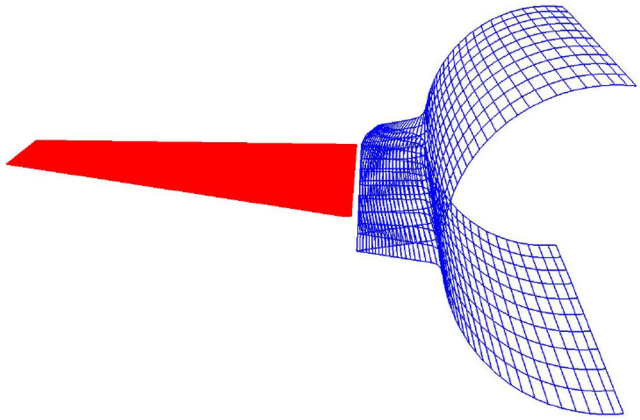

Fig. 7 CFD grid of the tail surface deflected in 2 deg relative to the fuselage surface.

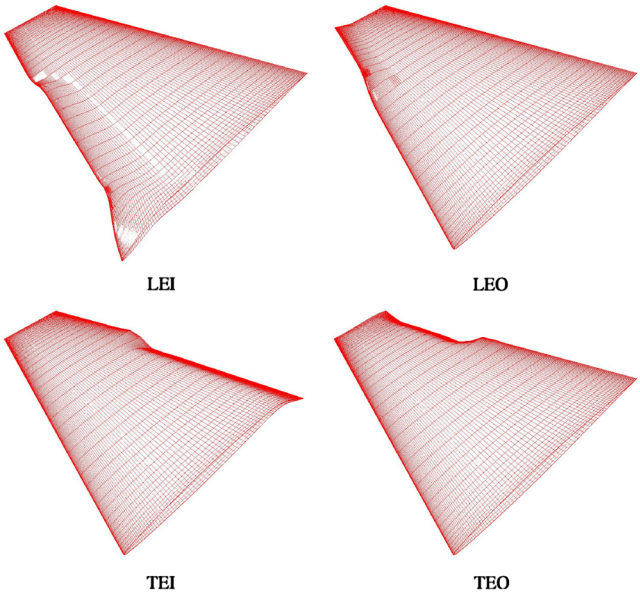

Fig. 8 Four flaps deflected to +20 deg.

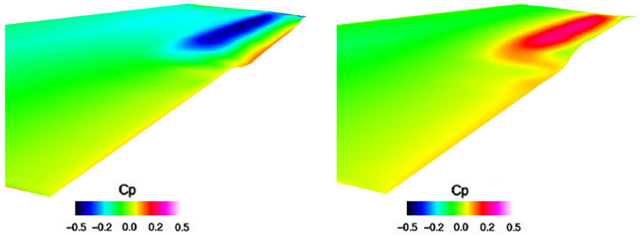

a) b)

Fig. 9 Pressure distribution on the upper wing surface with TEO flap deflected 10 deg down a) and 10 deg up b).

implementation of flap deformations, the CFD code is enhanced to read the locations of the flap hinges, and the flap deflection angles, as inputs. A set of auxiliary nodes is sparsely distributed on the wing and flap surface, as shown in Fig. 2b. These nodes are displaced according to the flap deflection, and the nodal displacements are mapped to the CFD surface grid using an IPS routine as implemented in [27].

The advantage of the IPS method is that it results in a smooth deflected mesh, independent of the flap position relative to the grid lines. Another advantage of the IPS method is that the same spline routines can be used both for representing the deflected flaps and for mapping elastic modes from the structural nodes to the CFD grids. Because for elastic analysis such a mapping routine is necessary, an IPS algorithm embedded within the CFD code can serve for both purposes.

Numerical Test Case

This section presents trim analyses of a fighterlike model, in two maneuvers: A 1-*g* level-flight maneuver, at Mach 0.5, sea level (SL), for the rigid and elastic aircraft configurations, and a 5-*g* pull-up maneuver, at Mach 0.8, SL, for an elastic aircraft configuration. Level-flight results are compared with those computed by ZAERO, using linear aerodynamics, for method verification. This section also presents the details associated with modeling and CFD analysis of deflected flaps.

Structural and Aerodynamic Models

The structural model of the aircraft used in this research is shown in Fig. 3. It is a Nastran preliminary-design finite element model of a generic aluminum fighter aircraft (AFA) that has been used in several aeroelastic studies [21,23]. It has four wing control surfaces, two along the trailing edge and two along the leading edge, a horizontal, all movable tail (HT), and a vertical tail. It corresponds to a wing with an aspect ratio of 4.8, a total planform area of 272 ft^2, a taper ratio of 30%, and a leading-edge sweep of 37 deg. The configuration weighs about 30,000 lbs. Ten elastic symmetric modes served as generalized coordinates in the trim analysis. The first four modes, with their associated frequencies, are presented in Fig. 4. Each mode is presented in the finite element coordinates, in which it was generated, in the left column. The two wire frames present the deformed and undeformed shapes. Figure 4 also presents the modes mapped to the linear panel model (middle column), and to the CFD surface grids (right column).

Maneuver trim analysis using ZAERO, based on a linear aerodynamic panel model, serves as a reference to the newly proposed trim method. The linear aerodynamic model is shown in Fig. 5. It is a ZAERO flat-panel model [28] containing 220 panels on the wing and its control surfaces, 42 panels on the horizontal tail, and 66 panels on the fuselage. It contains paneling for the horizontal tail and four wing control surfaces, which coincide with the control surfaces on the structural model.

The CFD code used in this study is the elastic zonal Navier–Stokes simulation (EZNSS) [29], a time-accurate implicit finite-differences code, based on the Beam and Warming algorithm. The code's inviscid Euler scheme is used to maintain the required computational resources within the limits of the resources available to the author. Figure 6 presents the CFD model. It comprises three computational zones, for the fuselage, wing, and horizontal tail, and an interface zone. The size of each grid zone is provided in Table 1. The total

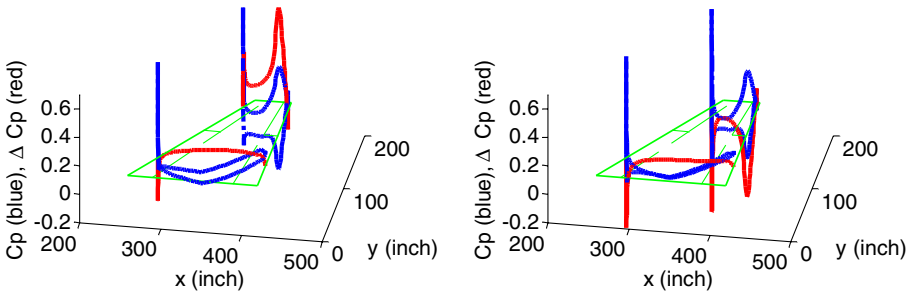

a) b)

Fig. 10 Pressure coefficient distribution at 30 and 70% span sections for the case of TEO flap deflected 10 deg down a) and 10 deg up b).

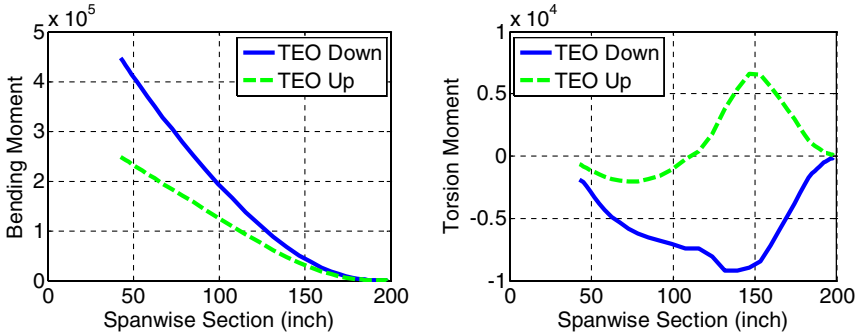

a) b)

Fig. 11 Spanwise bending a) and torsion b) moment distribution for the case of TEO flap deflected 10 deg up and down.

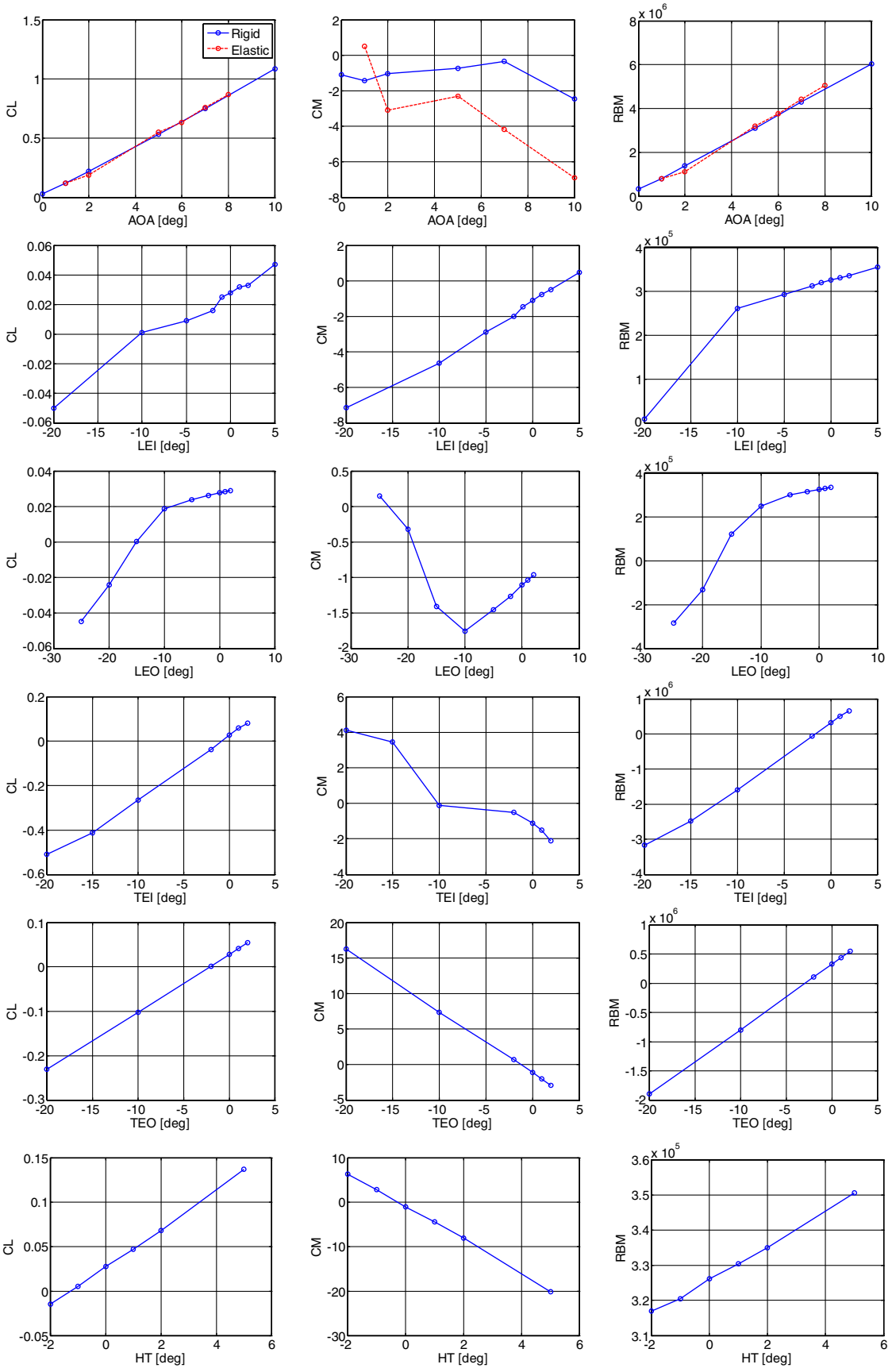

Fig. 12 Lift coefficient, pitching moment, and RBM vs trim parameters; Mach 0.8, SL.

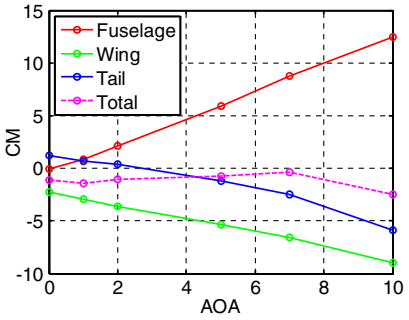

Fig. 13 Contribution to pitching moment of fuselage, wing, and HT; rigid configuration, Mach 0.8.

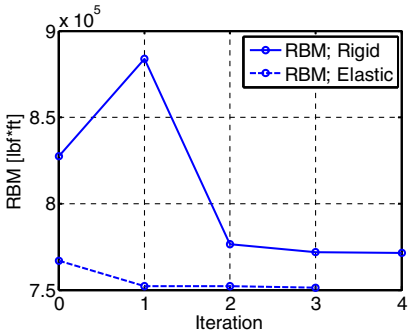

Fig. 16 RBM during trim analysis; 1-*g* level flight, Mach 0.5, sea level.

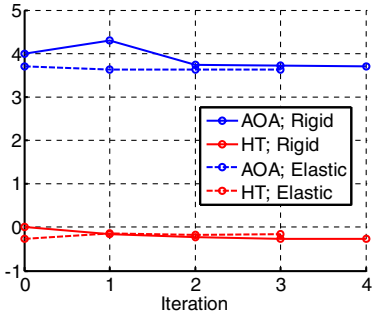

Fig. 14 Trim parameter values during trim analysis; 1-*g* level flight, Mach 0.5, sea level.

number of grid points of the model is about 1.4×10^6. The wing and HT have separate C-type meshes, which are embedded in the fuselage O-type grid zone, based on the Chimera grid method. The use of the Chimera overset grids makes it straightforward to tilt the HT, with its complete grid zone. The HT zone was modeled such that it is separate from the fuselage, as shown in Fig. 7. This allows for airflow through the gap between the fuselage and the HT, as in reality.

Deflected Flaps: Modeling and Flow Analysis

Four flaps are modeled. These are the leading-edge inboard (LEI), leading-edge outboard (LEO), trailing-edge inboard (TEI), and trailing-edge outboard (TEO) surfaces. Figure 8 presents the wing–flap surface grids with each of the four flaps deflected to 20 deg. Figure 8 demonstrates that flap deflections computed by the IPS method result in smooth grid surfaces, which are manageable by the CFD code.

An example of flow analysis with deflected flaps is presented in Figs. 9–11, for the rigid-wing case. Figure 9 presents pressure distribution over the wing's upper surface, for the cases of TEO flap (aileron) deflected 10 deg down and up, showing the perspective decrease and increase in upper-surface pressure on the flap. The flap was deflected about 0 deg AOA. Figure 10 presents the pressure coefficient on the upper and lower surfaces, at two wing sections, inboard to the flap and on the flap. The wing section inboard of the flap generates very little lift, while the flap section generates lift force, positive or negative, depending on the flap deflection. The center of pressure on the flap wing section is shifted rearward, in the chordwise direction.

Figure 11 presents the spanwise bending and torsion moment distribution for the cases of TEO flaps deflected 10 deg up and down. Positive, down deflection of the TEO flap increases the lift at the outboard wing thus increasing the root bending moment. It also shifts the chordwise center of pressure backward, creating a negative, nose-down torsion moment.

Sensitivity Derivatives

Baseline sensitivities were calculated by finite differences. The pitching-moment coefficient was calculated about the center of gravity, located at $x = 318.81$, $y = 0$, $z = 0$ (in.). The CFD-code convention is to compute the moment coefficients using a unit reference length. As a result, pitching-moment coefficients reported below are large figures, when compared to typical pitching-moment values. Figure 12 presents lift coefficients, moment coefficients, and RBM, vs trim parameters, for the rigid and elastic aircraft configurations, at Mach 0.8. The elastic parameters were computed based on SL ambient pressure. Figure 12 shows that at the range of trim parameters presented, the lift coefficient and RBM are approximately linear with the trim parameters, except for the case of LEO. Also, the pitching-moment coefficient varies somewhat nonlinearly with the AOA. This nonlinear behavior of the pitching moment is due to the opposite, and nonlinear, contributions of the fuselage (pitch up), and wing and HT (pitch down), as shown in Fig. 13. Therefore, the pitching-moment sensitivity value used at each trim optimization case was decided upon based on the estimated trim AOA.

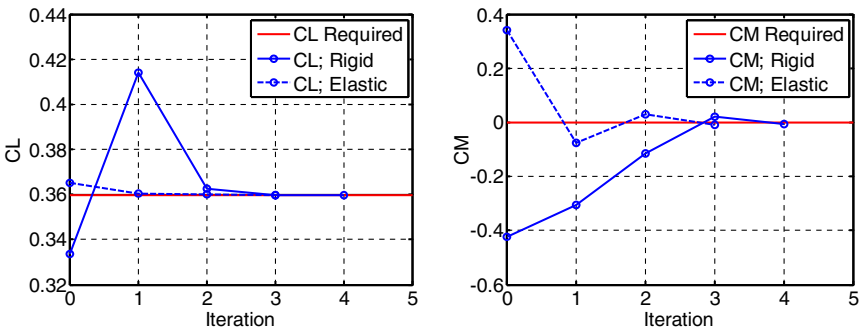

a) **b)**

Fig. 15 Lift a) and moment coefficient b) during trim analysis; 1-*g* level flight, Mach 0.5, sea level.

Table 2 Trim parameters and RBM; 1-*g* level flight, Mach 0.5, sea level

	AOA	HT	LEI	LEO	TEI	TEO	RBM, lb · in.
Traditional trim; rigid	3.7 deg	−0.3 deg	——	——	——	——	0.77E + 06
Trim optimization; rigid	5.0 deg	1.7 deg	3.0 deg	3.0 deg	−0.2 deg	−10.0 deg	0.54E + 06
Traditional trim; elastic	3.6 deg	−0.2 deg	——	——	——	——	0.75E + 06
Trim optimization; elastic	5.0 deg	0.5 deg	−10.0 deg	3.0 deg	−2.3 deg	−10.0 deg	0.59E + 06

Table 3 Trim parameters for 1-*g* level flight, Mach 0.5, sea level; computed by ZAERO

	AOA	HT	LEI	LEO	TEI	TEO	RBM, lb · in.
Traditional trim; rigid	3.7 deg	−0.7 deg	——	——	——	——	0.69E + 06
Trim optimization; rigid	5.0 deg	1.9 deg	3.0 deg	3.0 deg	−3.1 deg	−10.0 deg	0.41E + 05
Traditional trim; elastic	3.6 deg	−0.9 deg	——	——	——	——	0.70E + 06
Trim optimization; elastic	5.0 deg	1.3 deg	3.0 deg	−9.9 deg	−3.8 deg	−10.0 deg	0.45E + 05

Trim Analysis

The following sections present trim analysis of a 1-*g* level-flight maneuver, at Mach 0.5, SL, for the rigid and elastic aircraft configurations, controlling the maneuver with the AOA and HT only (traditional, determined trim system), and with all control surfaces (overdetermined trim system, trim optimization). Analysis of this plain maneuver, at a subsonic Mach number, and comparison with trim results obtained with ZAERO serve for method verification. Trim analysis is then presented for a 5-*g* pull-up maneuver, at Mach 0.8, SL, for an elastic aircraft configuration.

Traditional Trim Analysis—1 g Level Flight, Mach 0.5, Sea Level

Trim analyses of the rigid and elastic aircraft configurations were performed in iterations, according to the flowchart of Fig. 1: Trim parameters were computed based on the estimated *rigid* sensitivities. These parameters were input to an EZNSS flow analysis to compute their pertaining aerodynamic coefficients. A new set of trim parameters was computed, based on the differences between the CFD-computed and required lift- and pitching-moment coefficients. The process was repeated until the coefficients converged to their required trimmed values. Figures 14–16 present the trim parameters, aerodynamic coefficients, and RBM, respectively, at each trim iteration. RBM was not optimized in this trim analysis and is presented only as a reference value.

Figures 14–16 show that the rigid trim process converged within three to four trim iterations. The elastic trim, which was started from the rigid trimmed solution, required an additional two to three trim iterations to converge. In all analyses, 500 flow iterations were run between two consecutive trim updates, and, in the elastic case, 100 flow iterations were computed between two consecutive elastic shape updates. Five hundred CFD iterations require 1 h of run time on a parallel silicon graphics (SGI) machine using 16 R12000-type

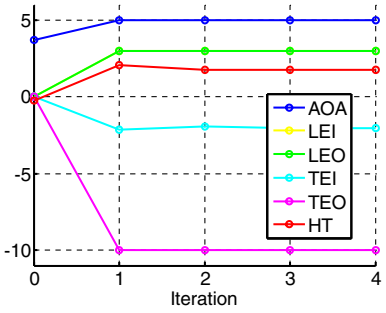

Fig. 17 Trim parameter values during trim optimization of the rigid aircraft; 1-*g* level flight, Mach 0.5, sea level.

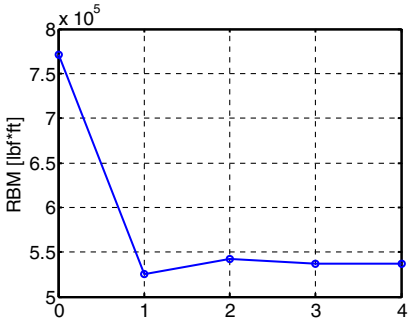

Fig. 19 RBM during trim optimization of the rigid aircraft ; 1-*g* level flight, Mach 0.5, sea level.

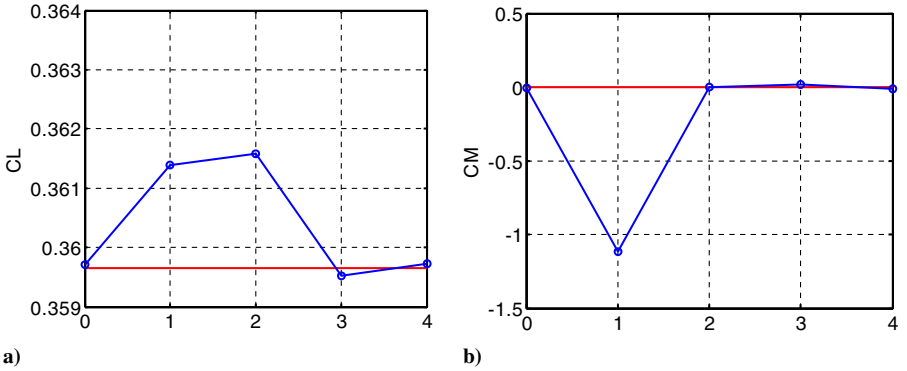

a) **b)**

Fig. 18 Lift a) and moment coefficient b) during trim optimization of the rigid aircraft ; 1-*g* level flight, Mach 0.5, sea level.

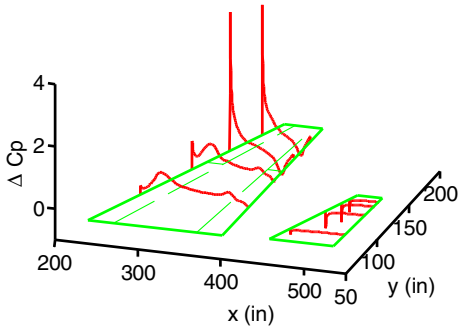

Fig. 20 Pressure coefficients on wing and tail sections at 20, 40, 60, and 80% of the span; trimmed rigid aircraft; 1-*g* level flight, Mach 0.5, sea level.

processors. Thus, the rigid and elastic trim analyses amounted to 1.5–2 and 1–1.5 h of run time, respectively.

Tables 2 and 3 present trim parameters and RBM values from the CFD-based trim analysis, and from trim analysis using ZAERO. Because the maneuver is performed at a subsonic Mach number and is associated with relatively small AOAs, it was speculated that a linear aerodynamic analysis can serve as a reference to the results obtained with the newly developed method. Comparison of trim parameter values indicates that for the traditional trim of the rigid configuration the two models resulted in the same trim AOA, and in a similar HT deflection. Differences in trim parameters are attributed to differences in the aerodynamic sensitivities, which may be a result of wing–wake tilt that is not captured with the panel model. This affects mainly the pitching moment due to AOA, and consequently the trim solution.

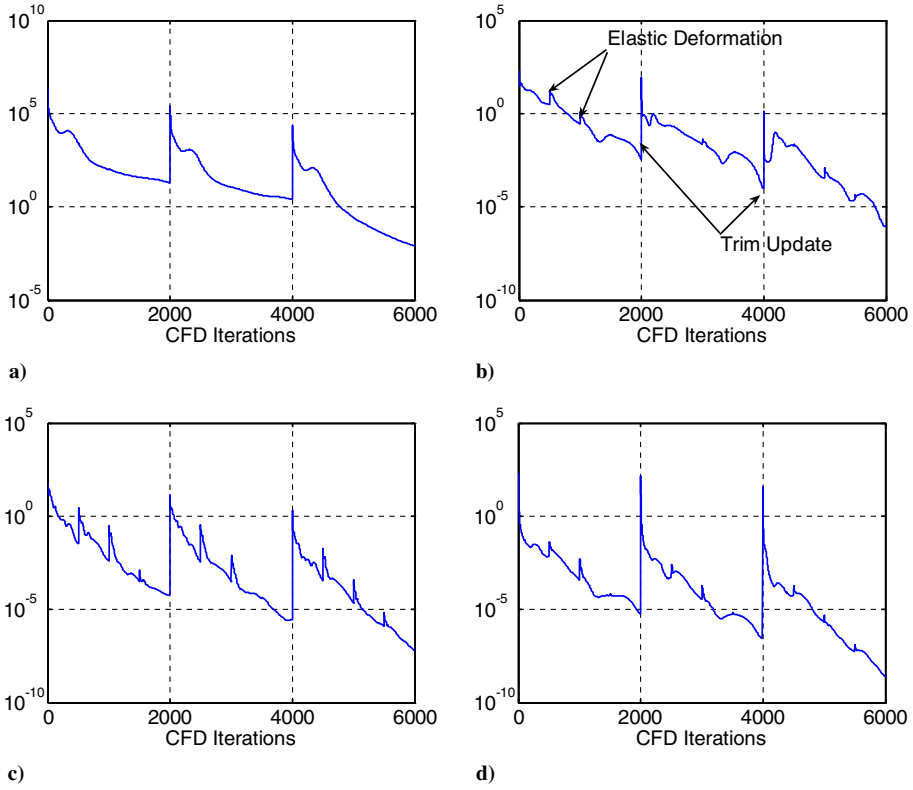

Fig. 21 CFD error (residual) during trim optimization of the elastic aircraft, at each computational zone: fuselage a), wing b), tail c), and interface zone d); 5-*g* pull-up, Mach 0.8, sea level.

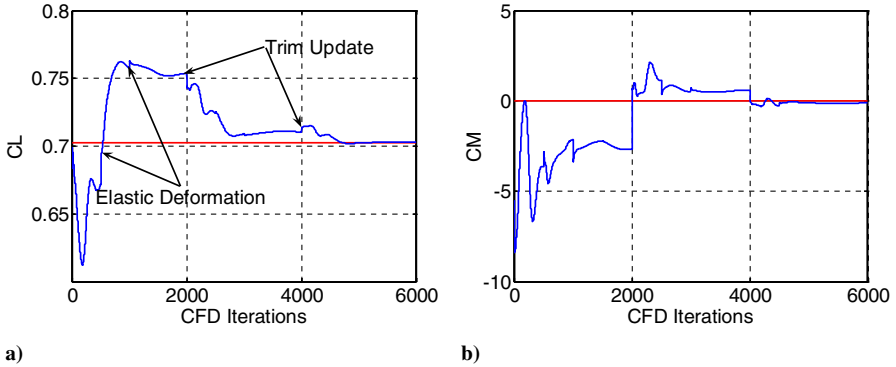

Fig. 22 Convergence of the lift a) and moment coefficient b) during trim optimization of the elastic aircraft; 5-*g* pull-up, Mach 0.8, sea level.

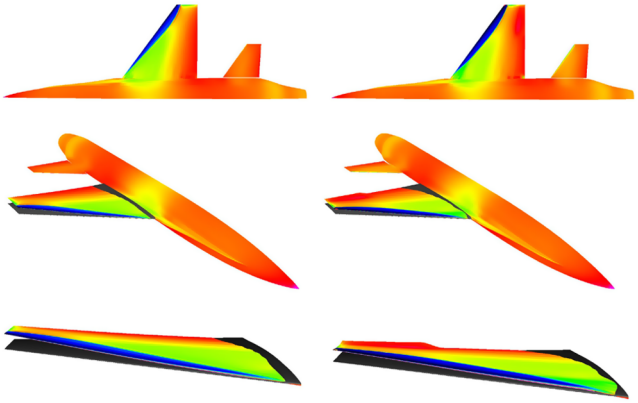

Fig. 23 Pressure distribution on the trimmed elastic aircraft; left column—traditional trim; right column—trim optimization with deflected wing control surfaces; 5-*g* pull-up, Mach 0.8, sea level.

Trim Optimization—1 g Level Flight, Mach 0.5, Sea Level

Figures 17–19, present trim parameters, aerodynamic coefficients, and RBM, respectively, at each trim iteration of the trim optimization process, for the rigid configuration. The AOA was limited to 5 deg, and the deflections of the leading-edge flaps were limited to positive 3 deg, to avoid large angles, which the flow solver is unable to compute. Trim optimization converged in four iterations, reducing the RBM by about 30%. The optimized trim parameter setting, detailed in Table 2, is such that lift is dumped off of the wing, especially off of the wing tip area, as seen in Fig. 20. This is achieved mainly by updeflection of the TEO surface (aileron).

Next, trim optimization of the 1-*g* level-flight maneuver was computed, accounting for elastic deformations. Trim parameters and RBM values are detailed in Table 2. RBM was reduced by over 20% compared to the traditional trim case value. It is noted, however, that the 1-*g* level-flight maneuver is not critical from the point of view of RBM value, and is used here only as a simple verification case for the CFD-based trim optimization process. Trim optimization has converged to the optimal trim parameters following four trim updates (not shown), and 2000 CFD iterations. Elastic deformations were performed following every 100 iterations. It is noted that trim optimization was performed based on the rigid sensitivities, yet the process converged at about the same rate as the rigid optimization process.

Comparison of the optimal trim parameters to those computed by ZAERO, as presented in Tables 2 and 3, show that the AOA, HT, and trailing-edge flap deflections are similar in the two analyses. The leading-edge flap deflections are, however, opposite. It is assumed that this is due to the known difficulty of linear panel codes to accurately capture the effects of shape alterations at the leading-edge area. Because the AFA wing is thin, and leading-edge suction is large, the CFD mesh is very fine at the leading-edge area. It is assumed that the effect of leading-edge flap deflections is captured more accurately in the CFD analysis than with the linear analysis.

Trim Analysis, Elastic Aircraft—5 g Pull-Up; Mach 0.8; SL

The benefits of CFD-based maneuver trim analysis manifests itself in the transonic flow regime, where the flowfield is dominated by shock waves that cannot be predicted by linear aerodynamic models. The next maneuver studied is a 5-*g* pull-up, at Mach 0.8, SL, elastic aircraft. Because the aircraft model is heavy weight, this maneuver is associated with large AOAs, about 7 deg (as detailed in Table 3), and moderate elastic structural deflections. For trim optimization, the AOA was limited to 7 deg, and the deflections of the leading-edge flaps were limited to positive 2 deg, to avoid large angles and detached flows, which the flow solver is unable to compute.

Trim optimization has converged within three trim iterations, applying 2000 CFD flow solver iterations between two consecutive trim iterations, and elastically deflecting the computational mesh every 500 CFD iterations. The starting point was the flowfield associated with 7 deg AOA and zero deflections of the control surfaces. Figure 21 presents convergence of the flowfield (CFD error) of each computational zone, showing the large increase in residual values following every trim parameters update, and the smaller jumps following elastic shape updates. Figure 22 presents convergence of the aerodynamic coefficients, during the trim optimization process. Figures 21 and 22 show that the elastic flowfield and aerodynamic coefficient values are roughly converged before each trim update is applied. This ensures a smooth convergence of the trim optimization process. Overall, this trim optimization process required 6000 CFD iterations, and 12 h of run time on a parallel SGI machine using 16 R12000-type processors.

Table 4 presents trim parameters and RBM values of the conventional and optimized trim analyses. Trim optimization resulted in the HT deflected positively, thus carrying some of the maneuver-required load, and reducing the load off of the wing. The TEO flap (aileron) is deflected upward to its maximum allowed deflection of 10 deg, dumping load off of the wing outboard section. As a result, the RBM of the optimized trim is about 15% lower than that of the traditional trim, and the elastic wing tip deflection is reduced by about 20% (shown in Fig. 23). Both trim cases resulted in a small wash-in deflection of the wing tip, of 0.5 and 0.4 deg for the traditional and optimized cases, respectively. Control surface hinge moments did not exceed their limits. The LEO hinge moment reached its limit of 10^6 (lb · in.).

Figure 23 presents pressure distribution on the trimmed, elastically deformed aircraft configuration, for the two trim cases. The upper view shows the formation of the lambda shock pattern on the wing. A noticeable feature of the newly presented trim scheme is that it provides accurate information on the pressure distribution, which is important for structural sizing, as well as for design of the control system.

Points to note regarding the trim optimization process are as follows:

1) In some cases it was found that the trim process is sensitive to convergence of the flow solutions between each two consecutive trim updates. In other words, trying to compute trim parameter updates based on nonconverged flowfield may result in divergence of the trim solution. This is due to the fact that one of the equality constraints requires a zero pitching-moment value. A slight deviation from zero value that is in the wrong direction may send the trim solution of the next trim iteration in the wrong direction.

2) Trim optimization can be carried out using the baseline rigid aerodynamic sensitivities, and there is no need to recompute them during the optimization process. This conclusion is currently shown only for the case of moderate elastic deformations, and has to be reevaluated in cases in which the elastic effects are pronounced. However, the fact that there is no need to recompute sensitivities significantly simplifies and shortens the trim procedure.

3) Using the minimization of RBM as an objective in maneuvers in which the RBM are not critical, as in the case of the level-flight maneuver, can lead to an illogical trim solution, in which the aircraft is maneuvering with almost no wing load (with the fuselage and HT carrying most of the maneuver load). A different trim optimization objective has to be defined in those cases. Because the newly developed trim tool is CFD based, the maneuver objective can be

Table 4 Trim parameters and RBM; 5-*g* pull-up, Mach 0.8, sea level

	AOA	HT	LEI	LEO	TEI	TEO	RBM, lb · in.
Traditional trim; elastic	6.3 deg	−0.7 deg	——	——	——	——	0.40E + 07
Trim optimization; elastic	6.6 deg	1.7 deg	2.0 deg	2.0 deg	0.6 deg	−10.0 deg	0.35E + 07

minimization of the drag forces, or a function that involves drag estimates.

Conclusions

A new method for CFD-based maneuver trim analysis and optimization was presented. The method belongs to the category of closely coupled aeroelastic analyses, in which the flow analysis, elastic deformations, and trim computations are performed within the CFD code, within a single run. The newly proposed methodology was successfully implemented within the EZNSS flow solver, and tested on a maneuvering fighterlike aircraft model. The maneuver simulations performed in the new tool consisted of a 1-*g* level flight at Mach 0.5, sea level, and a 5-*g* pull-up, at Mach 0.8, sea-level. Trim optimization objective of this study was chosen to be a minimization of root bending moments, with hinge moment constraints, and constraints on min and max values of the angle-of-attack, horizontal tail, and wing control surface deflections. The trim algorithm was found to be robust, and the closely coupled approach was found to be computationally efficient. Typical run times for the studied maneuvers are 2 and 12 h for the level flight and pull-up, respectively, on a parallel SGI machine using 16 R12000-type processors. The newly proposed methodology provides a tool for computing loads on a maneuvering realistic aircraft, in both traditional maneuver trim, and when wing control surfaces are used. It can be used to compute nonlinear maneuver loads, in the transonic flight regime, for structural design, and to gain insight on control laws that can be applied to reduce maneuver loads.

References

[1] Hacklinger, M., "The Development of Manoeuvre Load Criteria for Agile Aircraft," *AGARD Workshop on Design Loads for Advanced Fighters*, AGARD Rept. 746, Feb. 1988.

[2] Watson, G. J., "Eurofighter 2000 Structural Design Criteria and Design Loading Assumptions," *83rd Meeting of the AGARD Structures and Materials Panel, Florence, Italy*, AGARD Rept. 815, Sept. 1996.

[3] Gibson, D. H., "Evolution of F-16 Loads and Requirements," *83rd Meeting of the AGARD Structures and Materials Panel, Florence, Italy*, AGARD Rept. 815, Sept. 1996.

[4] Ausman, J., and Volk, J., "Integration of Flap Load Limiting into ASTROS," AIAA Paper 97-1115, 7–10 April 1997.

[5] Volk, J., and Ausman, J., "Integration of a Generic Flight Control System into ASTROS," AIAA Paper 96-1335, April 1996.

[6] Miller, G. D., "An Active Flexible Wing Multi-Disciplinary Design Optimization Method," AIAA Paper 94-4412, 7–9 Sept. 1994.

[7] Zillmer, S., "Integrated Multidisciplinary Optimization for Active Aeroelastic Wing Design," Air Force Wright Aeronautical Laboratories, WL-TR-97-3087, Aug. 1997.

[8] Zink, P. S., Mavris, D. N., and Raveh, D. E., "Maneuver Trim Optimization Techniques for Active Aeroelastic Wings," *Journal of Aircraft*, Vol. 38, No. 6, 2001, pp. 1139–1146.

[9] Zink, P. S., Raveh, D. E., and Mavris, D. N., "Robust Structural Design of an Active Aeroelastic Wing with Maneuver Load Uncertainty," *8th AIAA/USAF/NASA/ISSMO Symposium on Multidisciplinary Analysis and Optimization*, AIAA, Reston, VA, 6–8 Sept. 2000.

[10] Love, M., De La Garza, T., Charlton, E., and Eagle, D., "Computational Aeroelasticity in High Performance Aircraft Flight Loads," ICAS Paper 2000-4.8.1, 2000.

[11] Kingsley, G., Siegel, J. M., Jr., Harrans, V. J., Lawrence, C., and Luker, J. J., "Development of a Multi-Disciplinary Computing Environment (MDICE)," AIAA Paper 98-4738, Sept. 1998.

[12] Heinrich, R., Ahrem, R., Gunther, G., Kersken, H.-P., Kruger, W., and Neumann, J., "Aeroelastic Computation Using the AMANDA Simulation Environment," *Conference on Multidisciplinary Aircraft Design and Optimization*, CEAS, Germany, 2001.

[13] Stettner, M., Haase, W., Eberle, A., Grashof, J., and Schneider, M., "Coupled Static and Dynamic Aeroelastic Simulations in Transonic and Supersonic Flow," ICAS Paper 2000-4.8.2, 2000.

[14] Raveh, D., "Computational-Fluid-Dynamics-Based Aeroelastic Analysis and Structural Design Optimization—A Researcher's Perspective," *Computer Methods in Applied Mechanics and Engineering*, Vol. 194, Nos. 30–33, 2005, pp. 3453–3471. doi:10.1016/j.cma.2004.12.027

[15] Schuster, D. M., Vadyak, J., and Atta, E., "Static Aeroelastic Analysis of Fighter Aircraft Using a Three-Dimensional Navier-Stokes Algorithm," *Journal of Aircraft*, Vol. 27, No. 9, 1990, pp. 820–825.

[16] Schuster, D. M., "Application of a Navier-Stokes Aeroelastic Method to Improve Fighter Wing Performance at Maneuver Flight Conditions," *Journal of Aircraft*, Vol. 32, No. 1, 1995, pp. 77–83.

[17] Guruswamy, G. P., "Coupled Finite-Difference/Finite-Element Approach for Wing-Body Aeroelasticity," *Proceedings of the 4th Symposium on Multidisciplinary Analysis and Optimization*, AIAA, Washington, D.C., 1992, pp. 1–12.

[18] Obayashi, S., and Guruswamy, G. P., "Convergence Acceleration of Navier-Stokes Solver for Efficient Static Aeroelastic Computations," *AIAA Journal*, Vol. 33, No. 6, 1996, pp. 1134–1141.

[19] Raveh, D. E., Karpel, M., and Yaniv, S., "Nonlinear Design Loads for Maneuvering Elastic Aircraft," *Journal of Aircraft*, Vol. 37, No. 2, 2000, pp. 313–318.

[20] Raveh, D. E., and Karpel, M., "Structural Optimization of Flight Vehicles with Computational-Fluid-Dynamics-Based Maneuver Loads," *Journal of Aircraft*, Vol. 36, No. 6, 1999, pp. 1007–1015.

[21] Karpel, M., Moulin, B., and Love, M. H., "Modal-Based Structural Optimization with Static Aeroelastic and Stress Constraints," *Journal of Aircraft*, Vol. 34, No. 3, 1997, pp. 433–440.

[22] Raveh, D. E., Karpel, M., and Yaniv, S., "Nonlinear Design Loads for Maneuvering Elastic Aircraft," *Journal of Aircraft*, Vol. 37, No. 2, March–April 2000, pp. 313–318.

[23] Zink, P. S., Mavris, D. N., and Raveh, D. E., "Maneuver Trim Optimization Techniques for Active Aeroelastic Wings," *Journal of Aircraft*, Vol. 38, No. 6, Nov.–Dec. 2001, pp. 1139–1146.

[24] Goldin, Y., Levy, Y., and Arieli, R., "Wingtip Effects on Aileron Effectiveness," *44th Israel Annual Conference on Aerospace Sciences*, Technion IIT, Israel, Feb. 2004.

[25] Bartels, R. E., and Schuster, D. M., "Comparison of Two Navier-Stokes Aeroelastic Methods Using BACT Benchmark Experimental Data," AIAA Paper 99-3157, 1999.

[26] Harder, R. L., and Desmarais, R. N., "Interpolation Using Surface Splines," *Journal of Aircraft*, Vol. 9, No. 2, 1972, pp. 189–191.

[27] Raveh, D. E., and Karpel, M., "Structural Optimization of Flight Vehicles with Computational-Fluid-Dynamics-Based Maneuver Loads," *Journal of Aircraft*, Vol. 36, No. 6, 1999, pp. 1007–1015.

[28] ZAERO Theoretical Manual, Ver. 7, Chap. 3, ZONA Technology Inc., Scottsdale, AZ.

[29] Levy, Y., "Numerical Simulation of Dynamically Deforming Aircraft Configurations Using Overset Grids," *Journal of Aircraft*, Vol. 38, No. 2, 2001, pp. 349–354.